Diagnostic value of MRI proton density fat fraction for assessing liver steatosis in chronic viral C hepatitis

Poster No.:	C-0222
Congress:	ECR 2015
Type:	Scientific Exhibit
Authors:	R. Piccazzo[1], F. Paparo[1], L. Bacigalupo[1], M. Revelli[1], L. Cevasco[1], L.-P. Rollandi[1], A. Galletto[2], G. A. Rollandi[1]; [1]Genoa/IT, [2]Borgio Verezzi/IT
Keywords:	Tissue characterisation, Metabolic disorders, Infection, Technical aspects, Diagnostic procedure, Computer Applications-General, Ultrasound, MR, MR physics, Liver, Abdomen
DOI:	10.1594/ecr2015/C-0222

Aims and objectives

It is well known that hepatitis C virus (HCV), can lead to steatotic change in hepatocytes. In fact, the proportion of chronic hepatitis C patients with steatosis is considerable, suggesting a direct role of HCV in the intrahepatic accumulation of triglycerides [1, 2]. In addition, steatosis has been recognized as one of the factors capable of influencing both liver fibrosis progression and the rate of response to interferon-alpha-based therapy [3]. Currently, percutaneous liver biopsy remains the reference standard for the diagnosis and grading of hepatic steatosis, but its clinical application for purposes of screening, frequent monitoring, and epidemiologic studies is limited by the significant risk of bleeding, infection and sampling error [4]. Different non-invasive imaging techniques have been proposed to assess the presence and severity of hepatic steatosis, including ultrasonography (US), computed tomography (CT) and magnetic resonance imaging (MRI) [5]. Due to its power of tissue characterization, MRI has a pivotal role for the detection and quantification of liver fat content. To this regard, the main MRI-based tools include fat-suppressed and chemical-shift water-fat separation techniques, and magnetic resonance spectroscopy (MRS) [6-10]. Currently, MRS is regarded as the most accurate non-invasive imaging method for assessing fatty liver, and MRS-derived fat fraction (FF) represents an objective biomarker of this condition, characterized by a strong correlation with intracellular triglyceride content [11-16]. However, MRS is not widely available, is time consuming to perform and analyze, and samples only a small portion of the liver (i.e. a volume of about 4 cm3) [10, 12, 15]. Due to the limitations of spectroscopy, rapid chemical-shift methods are more commonly used in the clinical practice for estimating the liver FF [8, 11, 13, 17-19]. Otherwise, the application of these ready-available MRI techniques is hindered by the presence of different confounding factors (i.e. T1 relaxation effects, T2* decay, spectral complexity of fat, noise bias, B0 inhomogeneity and eddy currents), that require proper correction [10, 12, 18-20]. More recently, in order to eliminate all major biases seen with conventional chemical shift-based methods, newer multiecho [8, 11, 13, 21] and multi-interference [10, 12, 20, 22-24] methods incorporating spectral modeling of fat have been described for the quantification of proton density fat fraction (PDFF). In addition, in chronic liver disease, hepatic steatosis may coexist with various other histological abnormalities, including fibrosis, necroinflammatory activity, and hemosiderin deposition, which may act as confounding factors on fat quantification by MRI [8]. From a clinical viewpoint, the issue regarding MRI quantification of hepatic steatosis in patients affected by chronic viral C hepatitis has been addressed in few previous works [25-27]. The purpose of our study was to assess the diagnostic performance of an original T1-independent, T2*-corrected multiecho MRI technique for the estimation and quantification of liver steatosis in a cohort of patients with chronic viral C hepatitis, using histology as standard of reference, and assessing the influence of the other histological abnormalities on MRI PDFF measurements.

Methods and materials

Inclusion of patients

This was a prospective, monocentric, institutional review board approved study and patient's enrollment was performed at the Unit of Infectious Diseases of our Institution. From January 1st, 2013, through December 31st, 2013, 81 consecutive untreated patients with chronic viral C hepatitis were enrolled into the study after giving written informed consent. All patients were untreated (i.e. not under interferon-based therapies) at the time of enrollment. Exclusion criteria were the presence of major contraindications to 1.5T MRI (e.g. cardiac pacemaker, claustrophobia, foreign bodies and implanted medical devices with ferromagnetic properties [28]) and/or to liver biopsy (e.g. uncorrectable coagulopathy [29]). All included patients underwent MRI, transient elastography (TE) and liver biopsy within a time interval <10 days. Severe respiratory and motion artifacts on MR images were considered as an additional, post-MRI exclusion criteria to avoid unreliable measurements of MRI PDFF. After inclusion, the following laboratory values were obtained for all patients: aspartate aminotransferase (AST, expressed in IU/l), alanine transaminase (ALT, expressed in IU/L), gamma-glutamyl transpeptidase (GGT, expressed in IU/L), total bilirubin (expressed in mg/dL), platelet count (103 cells per µL of blood), and serum ferritin levels (expressed in ng/mL). Serum HCV-RNA levels were assessed in all patients by means of a quantitative method (real time polymerase chain reaction), and expressed in IU/mL.

MRI examinations and PDFF measurements

MRI of the liver was performed in the supine position on a 1.5T MRI scanner (Signa HDx, General Electric Medical Systems, Milwaukee, WI, USA) using a phased array, eight-element, flexible torso coil. All patients were carefully instructed to suspend respiration at the end of inspiration during the MRI sequence acquisition. A two-dimensional, spoiled, multiecho gradient-echo sequence with 16 echoes was performed in the axial plane to measure hepatic PDFF. The parameters of this sequence were adjusted in order to achieve a complete correction for confounding factors such as T1 bias, T2* decay, and water-fat signal interference [10, 12, 20]. To minimize T1 effects, a 20° flip angle was used at repetition time (TR) ranging from 120 to 270 msec, adjusted by the technologist to individual breath-hold capacity. To estimate water-fat signal interference and T2* effects, 16 echoes were obtained at serial opposed-phase and in-phase echo times (TE) (1.1, 2.25, 3.4, 4.55, 5.7, 6.85, 8, 9.15, 10.3, 11.45, 12.6, 13.75, 14.9, 16.05, 17.2, 18.35 msec) during a single breath hold of 12-34 seconds. Other imaging parameters were: 10 mm section thickness, 0 intersection gap, 125 kHz bandwidth, one signal average, and rectangular field of view with a 128×96 matrix adjusted to individual body habitus and breath-hold capacity. The multiecho gradient-echo MR images were exported in DICOM format for offline post-processing.

Image interpretation and data analysis

All MRI datasets derived from multiecho gradient-echo images were post-processed by a single experienced abdominal radiologist. The quantification of liver PDFF was performed with a publicly available software named C-Iron (Camelot Biomedical Systems SRL, Genoa, Italy; website: http://c-iron.camelotbio.com). C-Iron is a stand-alone software tool dedicated to the voxel-wise measurement of T2* decay for the quantification of iron overload and liver PDFF. Once acquired, the multiecho gradient-echo MR images are imported into the software. T2* values and PDFFs are estimated by fitting the MRI signal (S) acquired at different TEs with the following decay model proposed by Bydder et al. [20]:

$$|S(TE)| = \text{sqrt}\,[S_1^2 \exp(-2TE/T_{2,w}^*) + S2^2 \exp(-2TE/T_{2,f}^*) + 2\,S_1S_2 \exp(-TE/T_{2,w}^*) \exp(-TE/T_{2,f}^*) \cos(\#TE)]$$

where S1 and S2 are the signal amplitudes of water and fat respectively, T2,w* and T2,f* are the transverse relaxation times of water and fat, and #=2#/4.6 ms is the chemical shift between water and fat at 1.5T. The algorithm simultaneously estimates T2* and PDFF in each voxel of the image by using nonlinear least-squares fitting from all 16 echoes, assuming exponential decay and considering that fat has its own inherent T2 decay of 12 ms.

The quality of fit is assessed by means of the coefficient of determination R2 and pixels with low-quality fit are excluded from further processing by applying appropriate thresholds on the R2 value. The PDFF is then calculated by the following formula: $FF=S_2/(S_1+S_2)$.

A color-coded map reflecting the estimated PDFF values in each pixel of the image is displayed and juxtaposed on the corresponding axial MRI slice. The histogram of pixel distribution with mean, median and standard deviation of the PDFF values, is computed in a freehand, elliptical or rectangular user-adjustable ROI. A single abdominal radiologist, blinded to the results of both TE and histology, performed ROI positioning. A single freehand ROI was drawn in a mid-hepatic axial slice including the right lobe of the liver and systematically excluding large blood vessels, biliary ducts and focal lesions. The mean area of the ROIs was of about 40-60 cm2, depending on patient's anthropometric features (**Figure 1**). MRI PDFF and T2* decay were calculated in the same ROI. Clinically significant hepatic iron overload was defined by MRI T2* values less than 6.3 ms, corresponding to a liver iron concentration in dry tissue (LIC dry weight) of 4.2 mg/g [30, 31].

Transient elastography

Transient elastography (TE) is a corroborate method for the assessment of liver fibrosis in patients with chronic C hepatitis. TE was performed with FibroScan (Echosens, Paris, France) with liver stiffness measurements expressed in kiloPascals (values between 2.5 kPa and 75 kPa are expected) [32]. Acquisitions that do not have a correct vibration

shape or a correct follow-up of the vibration propagation are automatically rejected by the software. Measurements of liver stiffness were performed on the right lobe of the liver through intercostal spaces in correspondence to the mid-axillary line, while patients were lying in the supine position with the right arm in maximal abduction. In all included patients, TE measurements were successfully acquired (i.e. 10 correct measurements with an interquartile range lower than 30% of the median liver stiffness value [33]).

Liver biopsy

Ultrasound-assisted percutaneous liver biopsy was performed with an intercostal approach using 15- to 18-gauge needles. All biopsy specimens were fixed in formalin and embedded in paraffin. A single expert liver pathologist, blind to the results of both TE and MRI, read the specimens on site. Fibrosis was semi-quantitatively evaluated and staged on a 5-point scale from 0 to 4 according to the METAVIR scoring system (F0, absent; F1, enlarged fibrotic portal tract; F2, periportal or initial portal-portal septa but intact architecture; F3, architectural distortion but no obvious cirrhosis; and F4, cirrhosis) [34]. Necroinflammatory activity, represented by piecemeal necrosis and focal lobular necrosis, was semi-quantitatively evaluated by using the histological activity index described in the METAVIR system, and graded as follows: 0, no activity; 1, mild; 2, moderate; 3, severe [34, 35]. Liver steatosis was determined by estimating the percentage of fat-containing hepatocytes on haematoxylin-eosin stained specimens, and graded according to the method of Kleiner et al. [36]: S0, steatosis in fewer than 5% of hepatocytes; S1, 5%-33% of fatty hepatocytes; S2, 34%-66%; and S3, more than 66%. We also considered the percentage of fatty hepatocytes as an absolute value which was defined as histological fat fraction. Following the clinical standard, a Perl's Prussian blue reaction was applied to detect the presence of hemosiderin granules in biopsy specimens. The following ordinal 4-point scoring system was employed: grade 0, no iron deposits; grade 1, mild; grade 2, moderate; grade 3, high iron content [37].

Statistical analysis

Descriptive statistics were produced for demographic, clinical, and laboratory characteristics of patients. Categorical data were expressed as number and percentage, while continuous data as mean and standard deviation (SD), or median and range (from minimum to maximum). The normal distribution of different datasets was assessed by means of the D'Agostino-Pearson test. Nominal statistical significance was defined with a P of 0.05. The correlation of histological FF with MRI PDFF was tested by means of the Spearman's rank test, using both the arithmetic mean and the median of MRI PDFF values. Spearman's rho (r) values were interpreted as follows: for values of r of 0.9 to 1, the correlation is very strong; for values of r between 0.7 and 0.89, correlation is strong; for values of r between 0.5 and 0.69, correlation is moderate; for values of r between 0.3 and 0.4.9, correlation is moderate to low; for values of r between 0.16 and 0.29, correlation is weak to low; for values of r below 0.16, correlation is too low to be meaningful. Since the median MRI PDFF showed a better correlation with the histological FF, this parameter was adopted for the subsequent statistical analysis. The

correlation of median MRI PDFF values with histological FF was also tested using a partial correlation model, where liver stiffness, expressed in kPa, and T2* decay, expressed in ms, were introduced as confounding covariates. The cohort of patients was further stratified according to each histological feature of the METAVIR system, including fibrosis stage (F), inflammatory activity (A) and steatosis grade (S). Box plots were used to study the distribution of MRI PDFF according to each stage of fibrosis, inflammatory activity and steatosis, and the presence of significant differences in the median MRI PDFF values among subgroups of patients was tested using the non-parametrical Kruskal-Wallis test. After a positive Kruskal-Wallis test (p-value <0.05), a post-hoc analysis was conducted performing pairwise comparisons between subgroups. The diagnostic performance of MRI for detecting the correct histological grade of hepatic steatosis was assessed by using receiver operating characteristic (ROC) curves. For the ROC curve analysis, the area under curve (AUC), optimal cutoff values, sensitivity, specificity, positive and negative predictive values were calculated. Optimal cutoff values of MRI PDFF were chosen to maximize the sum of sensitivity and specificity for two steatosis thresholds: S0 vs S1-S2 (S#1) and S0-S1 versus S2 (S=2). Ultimately, the MRI PDFF was introduced as dependent variable in a multiple regression model, using patient's age, BMI, TE liver stiffness values, MRI T2* values, METAVIR stage of fibrosis, inflammation, steatosis, and histological FF as independent variables.

Images for this section:

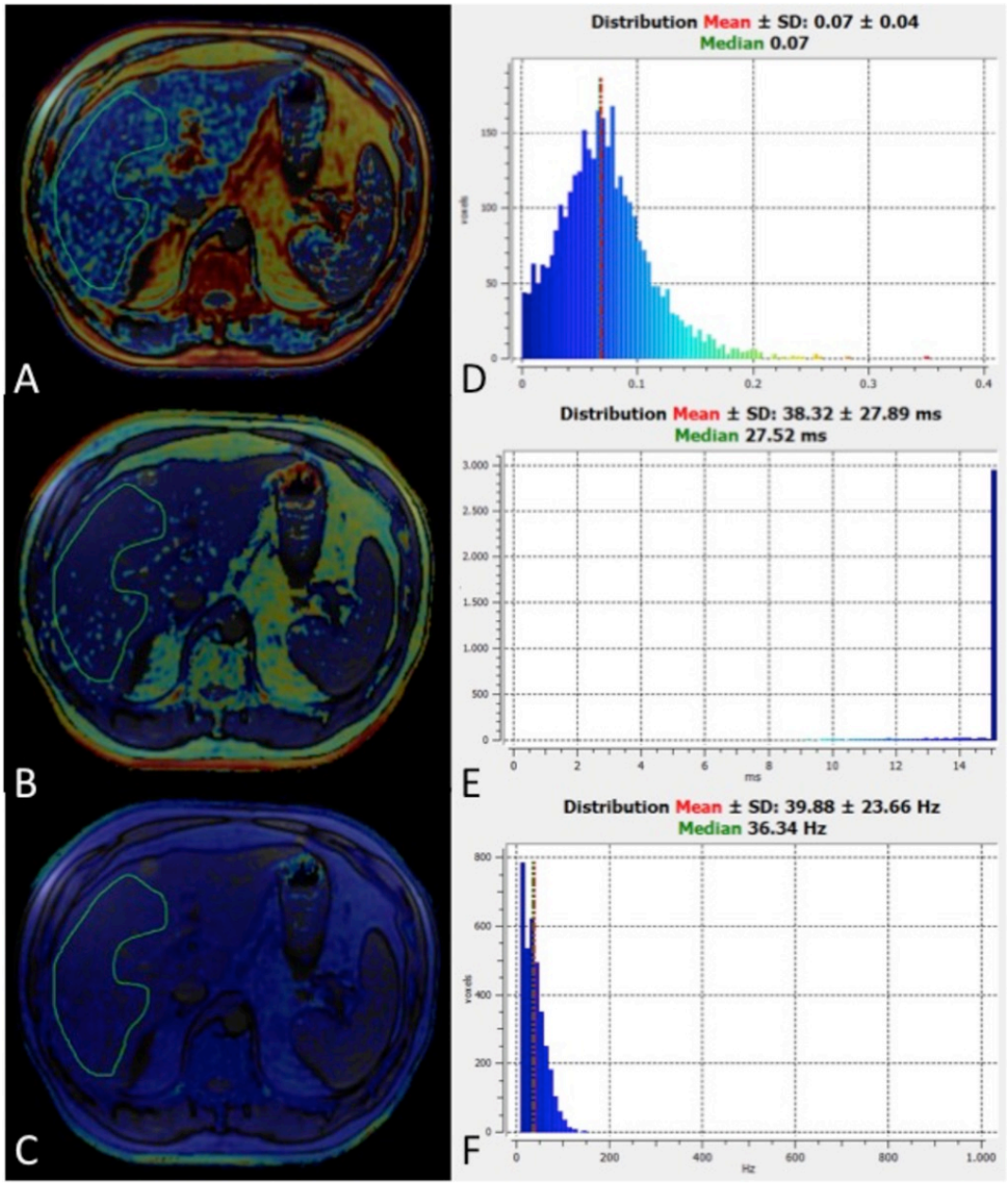

Fig. 1: Example of ROI positioning for the calculation of MRI PDFF (A), T2* (B) and R2* decay (reciprocal of T2*, expressed in Hz) (C) in a 52-year-old male patient with chronic viral C hepatitis. The histological FF of this patient was 10%, corresponding to a steatosis grade 1 (S1). Images D, E and F show the histogram of pixel distribution with mean values ± standard deviation and medians.

Results

Four patients were excluded due to severe motion/respiratory artifacts in their MRIs, precluding an accurate measurement of PDFF. The resulting cohort of 77 patients with chronic C hepatitis included 43/77 (55.8%) males and 34/77 (44.2%) females with a mean age of 51.31±11.27 (from 18 to 81) years and a mean BMI of 22.39±2.27 (from 18.43 to 27). Seventy-one/77 patients (92.2%) presented detectable serum HCV-RNA levels (above the detection threshold of 15 IU/mL of our method), while 6/77 patients (7.8%) were in sustained virological response. In this latter subgroup, the standard treatment with peginterferon and ribavirin was stopped at least 18 months before the time of inclusion. Demographic, clinical and laboratory characteristics of patients are summarized in (**Table 1**). The mean MRI PDFF of our cohort of patients, expressed in percentage units, was 11.76±4.73 with a median of 5.87 (from 0.7 to 17.01). The mean liver T2* value was 30.33±5.98 ms with a median of 31.32 ms (from 16.36 to 43.6 ms). We did not find patients with a histological steatosis of grade 3 (S3), and hemosiderin deposits were found in 4 patients. In addition, T2* values were not indicative of hepatic iron overload of clinical significance (i.e. below the threshold of 6.3 ms) in any patient. Therefore, we were not able to assess the diagnostic performance of MRI PDFF for the detection of severe steatosis (i.e. grade S3, >66% fat-containing hepatocytes), and the potential confounding effect of iron overload on MRI PDFF measurements. On the other hand, we introduced T2* values in the partial correlation model in order to verify their influence on the correlation between MRI PDFF and histological FF.

Correlation and subgroup analysis

The correlation of the mean MRI PDFF value with the histological FF was moderate (r=0.624, 95%CI for rho 0.465 to 0.744, p<0.0001), while the correlation of the median MRI PDFF value with the histological FF was strong (r=0.754, 95%CI for rho 0.637 to 0.836, p<0.0001). The median MRI PDFF values for each steatosis grade were: 4.3 (0.7-10.09) for S0; 10.4 (3.7-16.2) for S1; 13.5 (8.4-17.01) for S2 (p<0.05) (**Figures 2 and 3**). Stratifying the cohort of patients according to the METAVIR stages of parenchymal fibrosis, the median MRI PDFF values resulted significantly different among different subgroups (p<0.05 with the Kruskal-Wallis test). The post-hoc analysis showed that the median MRI PDFF in the F4 subgroup was significantly lower than in the other subgroups of patients (p<0.05) (**Table 2**). Stratifying the cohort of patients according to the METAVIR stages of necroinflammatory activity, the Kruskal-Wallis test did not reveal a significant difference among the median MRI PDFF values of the four subgroups of patients (p>0.05) (**Figure 4**). Box-and-whisker plots for MRI PDFF measurements in relation to each grade of steatosis, fibrosis and necroinflammatory activity are shown in **Figure 4**.

Diagnostic accuracy of MRI PDFF

The diagnostic accuracy of MRI PDFF evaluated by AUC-ROC analysis was 0.926 (standard error 0.0354, 95%CI 0.843 to 0.973) for S#1 and 0.929 (standard error 0.0363,

95%CI 0.847 to 0.975) for S=2. The best MRI PDFF cut-off value to differentiate between S0 vs. S1-S2 patients was 6.87, showing a sensitivity of 87.10% (95%CI 70.2-96.4), a specificity of 97.83 (95%CI 88.5-99.9%), a positive predictive value (PPV) of 96.4% (95%CI 81.7-99.9) and a negative predictive value (NPV) of 91.8% (95%CI 80.4-97.7) (**Figure 5A**). The best MRI PDFF cut-off value to differentiate between S0-S1 vs. S2 patients was 11.08, showing a sensitivity of 87.5% (95%CI 47.3-99.7), a specificity of 88.41% (95%CI 78.4-94.9), a positive predictive value (PPV) of 46.7% (95%CI 20.5-74.3) and a negative predictive value (NPV) of 98.4% (95%CI 91.3-100) **(Figure 5B**).

Influence of confounding variables on MRI PDFF measurements

The correlation between MRI PDFF and histological FF was strong even in a partial correlation model, using TE liver stiffness values (expressed in kPa) and T2* decay (expressed in ms) as covariates ($r=0.775$, $p<0.0001$).
The multiple regression analysis showed that only steatosis grade at histology and histological FF were factors independently associated to the median MRI PDFF (**Table 3**).

Images for this section:

Characteristics of patients	Proportions, Means ± Standard Deviation	Percentages, Medians and Range
Males	43/77	55.8%
Females	34/77	44.2%
Age	51.31±11.27	51 (18 – 81)
BMI	22.39±2.27	23 (18.43 – 27)
Serum AST level (U/L)	66.49±65.93	48 (18 – 293)
Serum ALT level (U/L)	62.83±53.13	51 (15 – 302)
Serum GGT level (U/L)	92.63±90.92	62 (11 – 368)
Total bilirubin (mg/dL)	1.05±1.26	0.7 (0.2 – 9)
Platelet count (10^3 cells/μL)	196.25±62.06	199 (99 – 462)
Serum ferritin level (ng/mL)	167.43±141.68	134.3 (13.3 – 700.4)
HCV-RNA (IU/mL)	1.96×106±1.91×106	1.34×106 (2.99×103–6.65×106)
Stiffness (kPa)	12.86±11.57	7.2 (3.8 – 55)
Histology		
Histological fat fraction	9.09±12.68	3 (0 – 45)
Steatosis grade (S)		
Grade 0 (<5%)	46/77	59.7%
Grade 1 (5-33%)	23/77	29.9%
Grade 2 (33-66%)	8/77	10.4%
Grade 3 (>66%)	0/77	0%
Necroinflammation (A)		
Grade 0	25/77	32.5%
Grade 1	33/77	42.8%
Grade 2	14/77	18.2%
Grade 3	5/77	6.5%
Fibrosis (F)		
F0 (none)	23/77	29.9%
F1 (Perisinusoidal or periportal)	14/77	18.2%
F2 (Perisinusoidal and portal/periportal)	12/77	15.5%
F3 (Bridging fibrosis)	18/77	23.4%
F4 (Cirrhosis)	10/77	13%
Histologically detectable iron		
Grade 0	73/77	94.8%
Grade 1	2/77	2.6%
Grade 2	2/77	2.6%
Grade 3	0/77	0%

Table 1: Characteristics of patients and results of histological analysis of liver biopsy specimens. Values are expressed as percentages, means ± standard deviation and medians (min - max). Legend: BMI, Body Mass Index.

Post-hoc analysis: distribution of PDFF according to METAVIR stages of fibrosis				
Factor	n	Median (range)	Average Rank	Pairwise comparisons with a significant result ($p<0.05$)
F0	23	6.7 (0.72–17.01)	44.61	F0 vs. F4
F1	14	6.7 (0.7–15.54)	43.25	F1 vs. F4
F2	12	6.07 (3.68-15.04)	40.33	F2 vs. F4
F3	18	5.78 (3.7–15.54)	39.36	F3 vs. F4
F4	10	3.43 (1.72–5.95)	17.90	F4 vs. F0/F1/F2/F3

Table 2: Distribution of MRI PDFF values according to different METAVIR stages of hepatic fibrosis. The Kruskal-Wallis test revealed a significant difference between groups ($p<0.05$). The post-hoc analysis demonstrates that the median MRI PDFF value of the F4 subgroup is significantly lower than that of the other subgroups of patients.

Regression Equation					
Independent variables	Coefficient	Std. Error	$r_{partial}$	t	P
(Constant)	8.3980				
Age	-0.01905	0.02438	-0.09435	-0.781	0.4372
BMI	-0.1480	0.1248	-0.1424	-1.186	0.2397
Necroinflammation (A)	0.07004	0.3184	0.02667	0.220	0.8266
Fibrosis (F)	-0.5041	0.3546	-0.1699	-1.422	0.1596
Steatosis (S)	2.3698	1.1144	0.2497	2.127	0.0371*
Liver stiffness	0.01464	0.04543	0.03903	0.322	0.7483
Histological FF	0.1325	0.05975	0.2597	2.218	0.0299*
T2*	0.03749	0.04626	0.09781	0.810	0.4205

Table 3: Multiple regression analysis. MRI PDFF is the dependent variable of the model. Histological FF and the histological grade of steatosis were the only two factors independently and significantly correlated to MRI PDFF. P-values below the level of statistical significance ($p<0.05$) are marked with the asterisk.

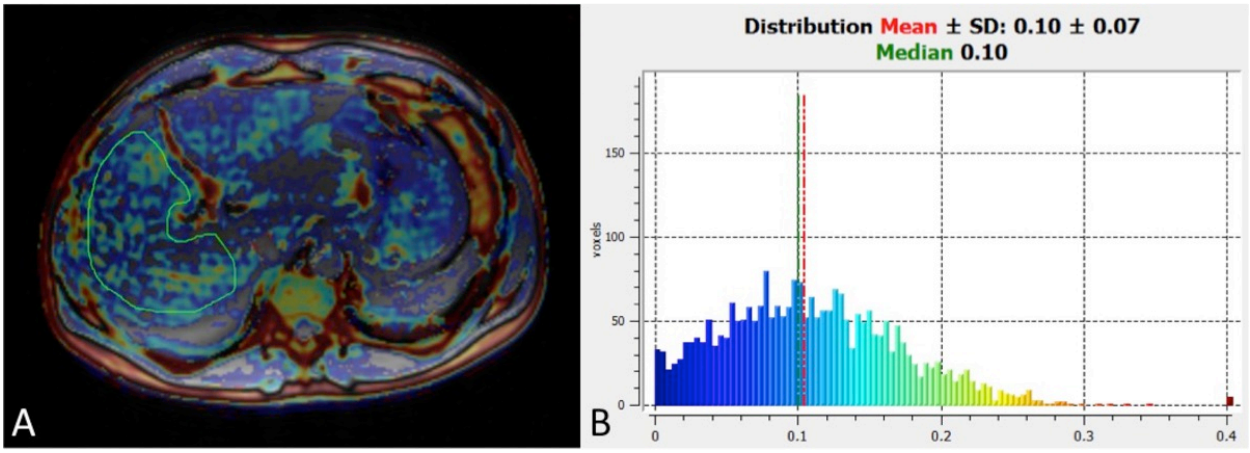

Fig. 2: Calculation of MRI PDFF in a 45-year-old male patient with chronic viral C hepatitis (A). The median MRI PDFF value is 10% (B), while histological FF of the patient was 8%, corresponding to a steatosis grade 1 (S1).

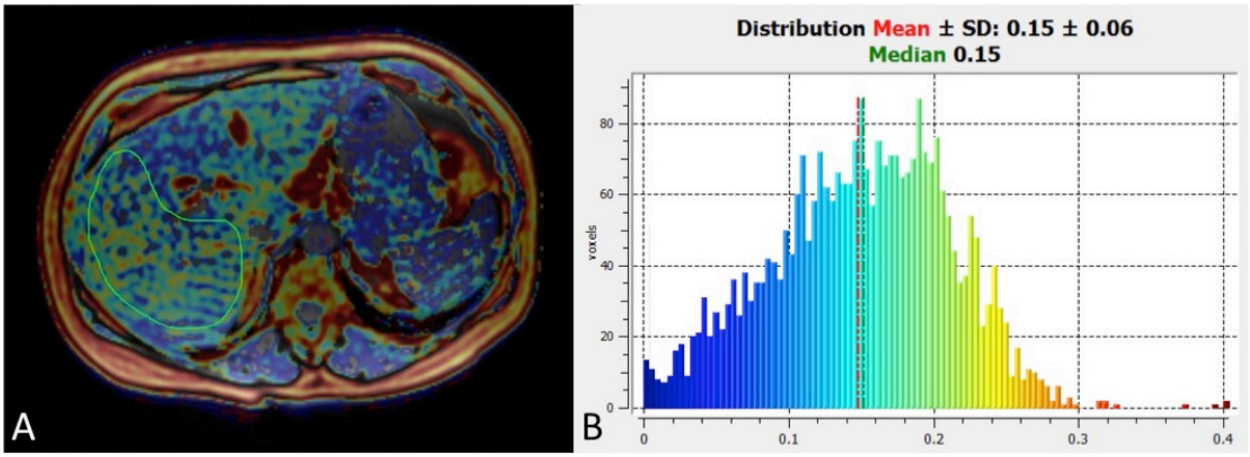

Fig. 3: Calculation of MRI PDFF in a 45-year-old male patient with chronic viral C hepatitis (A). The median MRI PDFF value is 15% (B), while histological FF of the patient was 37%, corresponding to steatosis grade 2 (S2).

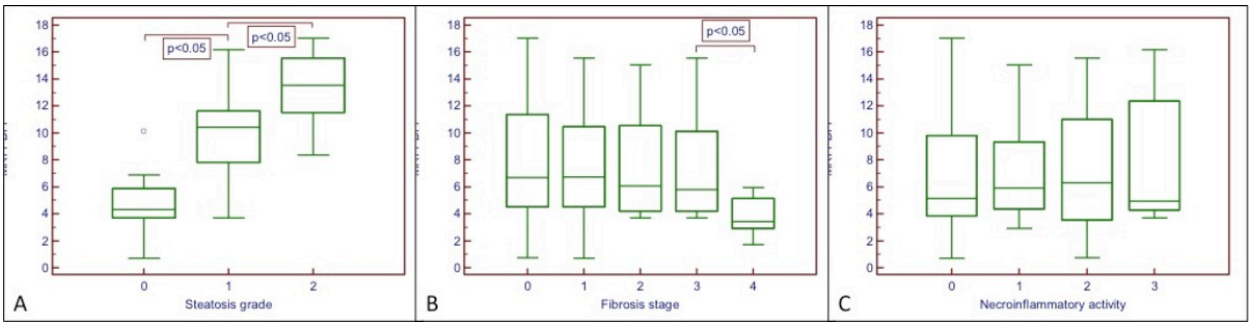

Fig. 4: Box-and-whisker plots for MRI PDFF measurements in relation to each grade of steatosis (A), fibrosis (B) and necroinflammatory activity (C). The top and the bottom of the boxes are the first and third quartiles, respectively. The length of the box represents the interquartile range including 50% of the values. The line through the middle of each box represents the median. The error shows the minimum and maximum values (range). An outside value (separate point) is defined as a value that is smaller than the lower quartile minus 1.5 times the interquartile range, or larger than the upper quartile plus 1.5 times the interquartile range.

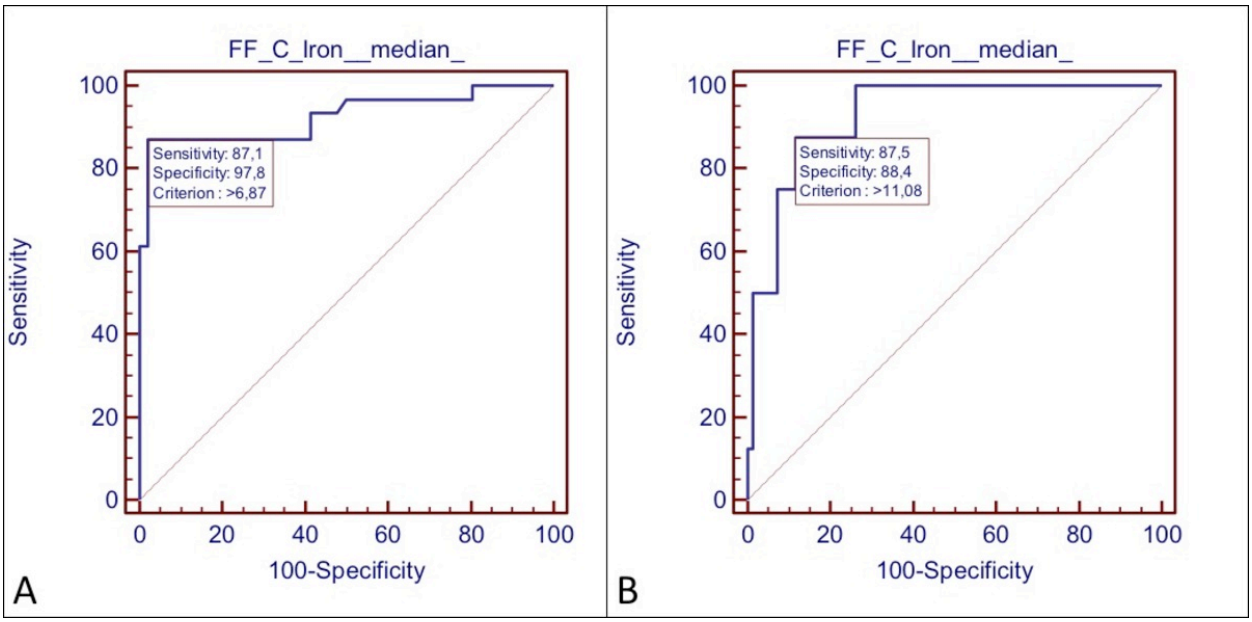

Fig. 5: ROC curve analysis of MRI PDFF for patients with steatosis S#1 (S0 vs S1-S2). The area under the ROC curve is 0.926 (95% CI 0.74-0.94) (A). ROC curve analysis of MRI PDFF for patients with steatosis S=2 (S0-S1 vs S2). The area under the ROC curve is 0.929 (95%CI 0.806 to 0.968) (B).

Conclusion

Liver biopsy with histological visualization of hepatocellular fat vacuoles remains the reference method in order to determine the grade of steatosis in chronic liver diseases, but it is an invasive procedure, which can study only a small portion of the liver (i.e. 1/50,000 of the total volume) [4, 31]. Discomfort and bleeding are well known procedure-related complications. In addition to sampling errors, routine histological examination is semi-quantitative, observer-dependent, and grading is performed with broad severity brackets [38]. Therefore, a non-invasive and objective assessment on a continuous scale may be preferable to biopsy in both clinical practice and research. Different non-invasive imaging methods, including US, CT and MRI, have been employed to provide an estimate of liver steatosis. It causes reduced liver attenuation at CT, resulting in low hepatic density compared to spleen during pre-contrast and portal venous phase imaging [5]. Despite the development of quantitative methods of image analysis to assess the severity of hepatic steatosis with CT [5], the clinical implementation of this imaging modality is hampered by exposure to ionizing radiation, which limits its application for repeated measurements in monitoring disease progression [9, 15]. Using B-mode US imaging, an indirect estimate of hepatic steatosis is obtained by comparing the echogenicity of the liver parenchyma with that of the cortex of the right kidney. This comparison may be performed in either semi-quantitative (i.e. normal liver echotexture, minimal, mild, moderate, severe hyperechogenicity [5]) or quantitative modality (i.e. hepatorenal index [39]). Hepatorenal index calculation has been presented as an effective tool for differentiating patients with steatosis from those without steatosis [39], showing a strong correlation with the histological FF ($r=0.71$, $p<0.0001$). However, it has to be kept in mind that a high echogenicity of the liver parenchyma in not synonymous of steatosis. In fact, this appearance of the liver at B-mode US may also be related to the presence of parenchymal fibrosis and liver iron overload, leading to overestimation of the true steatosis grade or misdiagnosis.

MRI-based techniques have been widely employed to determine the presence and grade the severity of hepatic steatosis, and MRS is regarded as the most accurate non-invasive method for assessing this condition [11-14]. In fact, FF calculated from spectroscopy-determined proton densities has shown a strong direct correlation with the intracellular triglyceride content [14, 15]. However, this expensive and time-consuming technique is not widely available and mainly limited to research settings. Advanced multiecho and multi-interference MRI techniques allow measurement of PDFFs that is corrected for confounding factors, including B0 inhomogeneity, T1 bias, T2* decay and multi-frequency signal interference effects caused by protons in fat [10-13, 18-20]. The most recent studies are giving encouraging results on clinical grounds, demonstrating a strong correlation between MRI PDFF and hepatic steatosis grade determined by histological validation and proposing MRI PDFF as a valid noninvasive biomarker for assessing liver fat content [22, 24]. In our work, we performed the quantification of MRI PDFF by means of a comprehensive model derived from that proposed by Bydder et al. [20], incorporating correction for T1- and T2* relaxation effects, B0 inhomogeneity and spectral

complexity of fat. This method of analysis has never been employed in a homogeneous cohort of patients with chronic C hepatitis. The prevalence of steatosis in chronic C hepatitis is about 40%, which represents an approximately 2-fold increase compared to the prevalence of steatosis in chronic B hepatitis (i.e. 20%) [1, 40]. According to the literature, we found in our cohort of patients a prevalence of steatosis of 40.26%. In HCV-related steatosis, the percentage of fat-containing hepatocytes is usually mild to moderate (i.e. 10-20%) [35], as it was observed in our study, with a median histological FF in patients with relevant steatosis (S#1) of 15%. In addition, we observed a lack of patients with grade 3 steatosis (i.e. >66% of fat-containing hepatocytes). The severity of steatosis seems to correlate with the level of HCV replication (i.e. HCV RNA levels in serum) [3], and it significantly reduces or disappears when patients are successfully treated with antivirals [41]. Interestingly, and according to our results, as the liver disease progresses to cirrhosis (i.e. F4 METAVIR stage of fibrosis), there is a trend of reduction of parenchymal steatosis [42], a phenomenon already observed in NAFLD [43]. Some longitudinal studies underscored the role of steatosis in fibrosis progression. In a recent study on paired liver biopsies performed in 135 untreated patients with chronic C hepatitis [44], steatosis was the only independent factor predictive of fibrosis progression. The progression of fibrosis was significantly related to the percentage of hepatocytes with steatosis [44]. Given the clinical importance of steatosis detection and grading in chronic viral C hepatitis, we aimed to assess the clinical value of MRI PDFF as a non-invasive biomarker of fatty liver, finding a significant, strong correlation of the MRI PDFF with the histological FF. According to the results of Tang et al. [10], we noticed that MRI PDFF values are lower than histological figures, and MRI PDFF cutoff values to distinguish between different steatosis grades are not comparable with the histological ones. This is not surprising, since histologic examination assesses the percentage of fat-containing cells in the biopsy specimens and does not measure the volumetric fat content in a wide portion of liver parenchyma. With MRI PDFF, the proportion of mobile protons contained within fat molecules of three-dimensional liver voxels is quantified [8, 10, 12]. Therefore, MRI PDFF and histological FF assess different aspects of steatosis.

Our study has some limitations. As mentioned above, the lack of patients with a grade 3 steatosis may be considered an intrinsic limitation when examining a cohort of patients affected by chronic viral C hepatitis. Therefore, we were not able to assess the diagnostic performance of PDFF for discriminating between S0-S2 vs. S3 patients. In addition, we did not find cases of clinically significant MRI-detectable iron overload (i.e. MRI T2* values <6.3 ms [30]), and the presence of hemosiderin deposits was appreciable in only few cases. This may be due to the low number of cirrhotic patients in our cohort; in fact, it is known that histologically detectable iron is more frequently associated with advanced parenchymal fibrosis and cirrhosis [45]. Therefore, we were not able to reliably assess the influence of hepatic iron accumulation on the MRI PDFF measurements. Nevertheless, we decided to introduce T2* decay as a confounding covariate in the partial correlation model, finding that its influence on the correlation between MRI PDFF and histological FF was not significant. A point of strength of our study is that we kept a reasonably low time-interval between MRI, liver biopsy and TE (<10 days), thus avoiding any meaningful change in the hepatic fat content during the biopsy-MRI imaging interim. In addition,

we performed a double check of the influence of parenchymal fibrosis on MRI PDFF measurements, introducing TE values of liver stiffness in the partial correlation model, and both TE values and METAVIR stage of fibrosis in the multiple linear regression analysis.

MRI PDFF is a promising technique for the non-invasive assessment of liver steatosis in patients with chronic viral C hepatitis. In particular, MRI PDFF has shown a strong correlation with the histological FF, and this correlation seems to be influenced by neither the stage of parenchymal fibrosis nor the necroinflammatory activity. In addition, MRI PDFF allows for discrimination between different histological grades of steatosis with good diagnostic accuracy. Further studies on larger cohort of patients involving adequate control groups are needed to get a complete clinical validation of this technique in patients with chronic viral C hepatitis.

References

1: Negro F. Mechanisms and significance of liver steatosis in hepatitis C virus infection. World J Gastroenterol. 2006 Nov 14;12(42):6756-65. Review. PubMed PMID: 17106922.
2: Asselah T, Rubbia-Brandt L, Marcellin P, Negro F. Steatosis in chronic hepatitis C: why does it really matter? Gut. 2006 Jan;55(1):123-30. Review. PubMed PMID: 16344578; PubMed Central PMCID: PMC1856395.
3: Adinolfi LE, Gambardella M, Andreana A, Tripodi MF, Utili R, Ruggiero G. Steatosis accelerates the progression of liver damage of chronic hepatitis C patients and correlates with specific HCV genotype and visceral obesity. Hepatology. 2001 Jun;33(6):1358-64. PubMed PMID: 11391523.
4: Fernández-Salazar L, Velayos B, Aller R, Lozano F, Garrote JA, González JM. Percutaneous liver biopsy: patients' point of view. Scand J Gastroenterol. 2011 Jun;46(6):727-31. doi:10.3109/00365521.2011.558112. Epub 2011 Mar 2. PubMed PMID: 21366386.
5: Qayyum A, Chen DM, Breiman RS, Westphalen AC, Yeh BM, Jones KD, Lu Y, Coakley FV, Callen PW. Evaluation of diffuse liver steatosis by ultrasound, computed tomography, and magnetic resonance imaging: which modality is best? Clin Imaging. 2009 Mar-Apr;33(2):110-5. doi: 10.1016/j.clinimag.2008.06.036. PubMed PMID: 19237053; PubMed Central PMCID: PMC2743961.
6: Reeder SB, Cruite I, Hamilton G, Sirlin CB. Quantitative Assessment of Liver Fat with Magnetic Resonance Imaging and Spectroscopy. J Magn Reson Imaging. 2011 Oct;34(4):spcone. PubMed PMID: 22025886; PubMed Central PMCID: PMC3177109.
7: Wu CH, Ho MC, Jeng YM, Hsu CY, Liang PC, Hu RH, Lai HS, Shih TT. Quantification of hepatic steatosis: a comparison of the accuracy among multiple magnetic resonance techniques. J Gastroenterol Hepatol. 2014 Apr;29(4):807-13. doi: 10.1111/jgh.12451. PubMed PMID: 24224538.
8: Kang BK, Yu ES, Lee SS, Lee Y, Kim N, Sirlin CB, Cho EY, Yeom SK, Byun JH, Park SH, Lee MG. Hepatic fat quantification: a prospective comparison of magnetic resonance spectroscopy and analysis methods for chemical-shift gradient echo magnetic resonance imaging with histologic assessment as the reference standard. Invest Radiol. 2012 Jun;47(6):368-75. doi: 10.1097/RLI.0b013e31824baff3. PubMed PMID: 22543969.
9: Bohte AE, van Werven JR, Bipat S, Stoker J. The diagnostic accuracy of US, CT, MRI and 1H-MRS for the evaluation of hepatic steatosis compared with liver biopsy: a meta-analysis. Eur Radiol. 2011 Jan;21(1):87-97. doi: 10.1007/s00330-010-1905-5. Epub 2010 Jul 31. PubMed PMID: 20680289; PubMed Central PMCID: PMC2995875.
10: Tang A, Tan J, Sun M, Hamilton G, Bydder M, Wolfson T, Gamst AC, Middleton M, Brunt EM, Loomba R, Lavine JE, Schwimmer JB, Sirlin CB. Nonalcoholic fatty liver disease: MR imaging of liver proton density fat fraction to assess hepatic steatosis. Radiology. 2013 May;267(2):422-31. doi: 10.1148/radiol.12120896. Epub 2013 Feb 4. PubMed PMID: 23382291; PubMed Central PMCID: PMC3632805.
11: Yokoo T, Bydder M, Hamilton G, Middleton MS, Gamst AC, Wolfson T, Hassanein T, Patton HM, Lavine JE, Schwimmer JB, Sirlin CB. Nonalcoholic fatty liver disease:

diagnostic and fat-grading accuracy of low-flip-angle multiecho gradient-recalled-echo MR imaging at 1.5 T. Radiology. 2009 Apr;251(1):67-76. doi:10.1148/radiol.2511080666. Epub 2009 Feb 12. PubMed PMID: 19221054; PubMed Central PMCID: PMC2663579.
12: Meisamy S, Hines CD, Hamilton G, Sirlin CB, McKenzie CA, Yu H, Brittain JH, Reeder SB. Quantification of hepatic steatosis with T1-independent, T2-corrected MR imaging with spectral modeling of fat: blinded comparison with MR spectroscopy. Radiology. 2011 Mar;258(3):767-75. doi: 10.1148/radiol.10100708. Epub 2011 Jan 19. PubMed PMID: 21248233; PubMed Central PMCID: PMC3042638.
13: Guiu B, Petit JM, Loffroy R, Ben Salem D, Aho S, Masson D, Hillon P, Krause D, Cercueil JP. Quantification of liver fat content: comparison of triple-echo chemical shift gradient-echo imaging and in vivo proton MR spectroscopy. Radiology. 2009 Jan;250(1):95-102. doi:10.1148/radiol.2493080217. PubMed PMID: 19092092.
14: Mehta SR, Thomas EL, Bell JD, Johnston DG, Taylor-Robinson SD. Non-invasive means of measuring hepatic fat content. World J Gastroenterol. 2008 Jun 14;14(22):3476-83. PubMed PMID: 18567074; PubMed Central PMCID: PMC2716608.
15: Awai HI, Newton KP, Sirlin CB, Behling C, Schwimmer JB. Evidence and recommendations for imaging liver fat in children, based on systematic review. Clin Gastroenterol Hepatol. 2014 May;12(5):765-73. doi:10.1016/j.cgh.2013.09.050. Epub 2013 Sep 30. PubMed PMID: 24090729; PubMed Central PMCID: PMC3969892.
16: Lee SS, Park SH, Kim HJ, Kim SY, Kim MY, Kim DY, Suh DJ, Kim KM, Bae MH, Lee JY, Lee SG, Yu ES. Non-invasive assessment of hepatic steatosis: prospective comparison of the accuracy of imaging examinations. J Hepatol. 2010 Apr;52(4):579-85. doi:10.1016/j.jhep.2010.01.008. Epub 2010 Feb 2. PubMed PMID:20185194.
17: Fischer MA, Nanz D, Reiner CS, Montani M, Breitenstein S, Leschka S, Alkadhi H, Stolzmann P, Marincek B, Scheffel H. Diagnostic performance and accuracy of 3-D spoiled gradient-dual-echo MRI with water- and fat-signal separation in liver-fat quantification: comparison to liver biopsy. Invest Radiol. 2010 Aug;45(8):465-70. doi: 10.1097/RLI.0b013e3181da1343. PubMed PMID: 20479652.
18: Kühn JP, Evert M, Friedrich N, Kannengiesser S, Mayerle J, Thiel R, Lerch MM, Dombrowski F, Mensel B, Hosten N, Puls R. Noninvasive quantification of hepatic fat content using three-echo dixon magnetic resonance imaging with correction for T2* relaxation effects. Invest Radiol. 2011 Dec;46(12):783-9. doi:10.1097/RLI.0b013e31822b124c. PubMed PMID: 21808200.
19: Henninger B, Kremser C, Rauch S, Eder R, Judmaier W, Zoller H, Michaely H, Schocke M. Evaluation of liver fat in the presence of iron with MRI using T2* correction: a clinical approach. Eur Radiol. 2013 Jun;23(6):1643-9. doi:10.1007/s00330-012-2745-2. Epub 2013 Jan 19.
20: Bydder M, Yokoo T, Hamilton G, Middleton MS, Chavez AD, Schwimmer JB, Lavine JE, Sirlin CB. Relaxation effects in the quantification of fat using gradient echo imaging. Magn Reson Imaging. 2008 Apr;26(3):347-59. Epub 2008 Feb 21. PubMed PMID: 18093781; PubMed Central PMCID: PMC2386876.
21: Yu H, McKenzie CA, Shimakawa A, Vu AT, Brau AC, Beatty PJ, Pineda AR, Brittain JH, Reeder SB. Multiecho reconstruction for simultaneous water-fat

decomposition and T2* estimation. J Magn Reson Imaging. 2007 Oct;26(4):1153-61. PubMed PMID:17896369.
22: Idilman IS, Aniktar H, Idilman R, Kabacam G, Savas B, Elhan A, Celik A, Bahar K, Karcaaltincaba M. Hepatic steatosis: quantification by proton density fat fraction with MR imaging versus liver biopsy. Radiology. 2013 Jun;267(3):767-75. doi:10.1148/radiol.13121360. Epub 2013 Feb 4. PubMed PMID: 23382293.
23: Yu H, Shimakawa A, McKenzie CA, Brodsky E, Brittain JH, Reeder SB. Multiecho water-fat separation and simultaneous R2* estimation with multifrequency fat spectrum modeling. Magn Reson Med. 2008 Nov;60(5):1122-34. doi:10.1002/mrm.21737. PubMed PMID: 18956464; PubMed Central PMCID: PMC3070175.
24: Idilman IS, Keskin O, Elhan AH, Idilman R, Karcaaltincaba M. Impact of sequential proton density fat fraction for quantification of hepatic steatosis in nonalcoholic fatty liver disease. Scand J Gastroenterol. 2014 May;49(5):617-24. doi: 10.3109/00365521.2014.894118. Epub 2014 Apr 2. PubMed PMID: 24694249.
25: Ghotb A, Noworolski SM, Madden E, Scherzer R, Qayyum A, Pannell J, Ferrell L, Peters M, Tien PC. Adipose tissue and metabolic factors associated with steatosis in HIV/HCV coinfection: histology versus magnetic resonance spectroscopy. J Acquir Immune Defic Syndr. 2010 Oct;55(2):228-31. doi: 10.1097/QAI.0b013e3181e1d963. PubMed PMID: 20512045; PubMed Central PMCID: PMC2943991.
26: Mitchell DG, Navarro VJ, Herrine SK, Bergin D, Parker L, Frangos A, McCue P, Rubin R. Compensated hepatitis C: unenhanced MR imaging correlated with pathologic grading and staging. Abdom Imaging. 2008 Jan-Feb;33(1):58-64. PubMed PMID: 17387539.
27: Orlacchio A, Bolacchi F, Cadioli M, Bergamini A, Cozzolino V, Angelico M, Simonetti G. Evaluation of the severity of chronic hepatitis C with 3-T1H-MR spectroscopy. AJR Am J Roentgenol. 2008 May;190(5):1331-9. doi: 10.2214/AJR.07.2262. PubMed PMID: 18430852.
28: Dewey M, Schink T, Dewey CF. Frequency of referral of patients with safety-related contraindications to magnetic resonance imaging. Eur J Radiol. 2007 Jul;63(1):124-7. Epub 2007 Mar 23. PubMed PMID: 17383136.
29: Thampanitchawong P, Piratvisuth T. Liver biopsy:complications and risk factors. World J Gastroenterol. 1999 Aug;5(4):301-304. PubMed PMID: 11819452.

30: Angelucci E, Giovagnoni A, Valeri G, Paci E, Ripalti M, Muretto P, McLaren C, Brittenham GM, Lucarelli G. Limitations of magnetic resonance imaging in measurement of hepatic iron. Blood. 1997 Dec 15;90(12):4736-42. PubMed PMID:9389689.
31: Paparo F, Cevasco L, Zefiro D, Biscaldi E, Bacigalupo L, Balocco M, Pongiglione M, Banderali S, Forni GL, Rollandi GA. Diagnostic value of real-time elastography in the assessment of hepatic fibrosis in patients with liver iron overload. Eur J Radiol. 2013 Dec;82(12):e755-61. doi:10.1016/j.ejrad.2013.08.038. Epub 2013 Aug 30. PubMed PMID: 24050879.
32: Sandrin L, Fourquet B, Hasquenoph JM, Yon S, Fournier C, Mal F, Christidis C, Ziol M, Poulet B, Kazemi F, Beaugrand M, Palau R. Transient elastography: a new noninvasive method for assessment of hepatic fibrosis. Ultrasound Med Biol. 2003 Dec;29(12):1705-13. PubMed PMID: 14698338.

33: Ziol M, Handra-Luca A, Kettaneh A, Christidis C, Mal F, Kazemi F, de Lédinghen V, Marcellin P, Dhumeaux D, Trinchet JC, Beaugrand M. Noninvasive assessment of liver fibrosis by measurement of stiffness in patients with chronic hepatitis C. Hepatology. 2005 Jan;41(1):48-54. PubMed PMID: 15690481.
34: Bedossa P, Poynard T. An algorithm for the grading of activity in chronic hepatitis C. The METAVIR Cooperative Study Group. Hepatology. 1996 Aug;24(2):289-93. PubMed PMID: 8690394.
35: Theise ND. Liver biopsy assessment in chronic viral hepatitis: a personal, practical approach. Mod Pathol. 2007 Feb;20 Suppl 1:S3-14. Review. PubMed PMID:17486049.
36: Kleiner DE, Brunt EM, Van Natta M, Behling C, Contos MJ, Cummings OW, Ferrell LD, Liu YC, Torbenson MS, Unalp-Arida A, Yeh M, McCullough AJ, Sanyal AJ; Nonalcoholic Steatohepatitis Clinical Research Network. Design and validation of a histological scoring system for nonalcoholic fatty liver disease. Hepatology. 2005 Jun;41(6):1313-21. PubMed PMID: 15915461.
37: Bülow R, Mensel B, Meffert P, Hernando D, Evert M, Kühn JP. Diffusion-weighted magnetic resonance imaging for staging liver fibrosis is less reliable in the presence of fat and iron. Eur Radiol. 2013 May;23(5):1281-7. doi:10.1007/s00330-012-2700-2. Epub 2012 Nov 9. PubMed PMID: 23138385.
38: Bedossa P, Dargère D, Paradis V. Sampling variability of liver fibrosis in chronic hepatitis C. Hepatology. 2003 Dec;38(6):1449-57. PubMed PMID: 14647056.
39: Marshall RH, Eissa M, Bluth EI, Gulotta PM, Davis NK. Hepatorenal index as an accurate, simple, and effective tool in screening for steatosis. AJR Am J Roentgenol. 2012 Nov;199(5):997-1002. doi: 10.2214/AJR.11.6677. PubMed PMID:23096171.
40: Rubbia-Brandt L, Quadri R, Abid K, Giostra E, Malé PJ, Mentha G, Spahr L, Zarski JP, Borisch B, Hadengue A, Negro F. Hepatocyte steatosis is a cytopathic effect of hepatitis C virus genotype 3. J Hepatol. 2000 Jul;33(1):106-15. PubMed PMID: 10905593.

41: Kumar D, Farrell GC, Fung C, George J. Hepatitis C virus genotype 3 is cytopathic to hepatocytes: Reversal of hepatic steatosis after sustained therapeutic response. Hepatology. 2002 Nov;36(5):1266-72. PubMed PMID: 12395339.
42: Rubbia-Brandt L, Fabris P, Paganin S, Leandro G, Male PJ, Giostra E, Carlotto A, Bozzola L, Smedile A, Negro F. Steatosis affects chronic hepatitis C progression in a genotype specific way. Gut. 2004 Mar;53(3):406-12. PubMed PMID:14960525; PubMed Central PMCID: PMC1773989.
43: Abdelmalek M, Ludwig J, Lindor KD. Two cases from the spectrum of nonalcoholic steatohepatitis. J Clin Gastroenterol. 1995 Mar;20(2):127-30. PubMed PMID:7769192.
44: Fartoux L, Chazouillères O, Wendum D, Poupon R, Serfaty L. Impact of steatosis on progression of fibrosis in patients with mild hepatitis C. Hepatology. 2005 Jan;41(1):82-7. PubMed PMID: 15690484.
45: Pirisi M, Scott CA, Avellini C, Toniutto P, Fabris C, Soardo G, Beltrami CA, Bartoli E. Iron deposition and progression of disease in chronic hepatitis C. Role of interface hepatitis, portal inflammation, and HFE missense mutations. Am J Clin Pathol. 2000 Apr;113(4):546-54. PubMed PMID: 10761457.